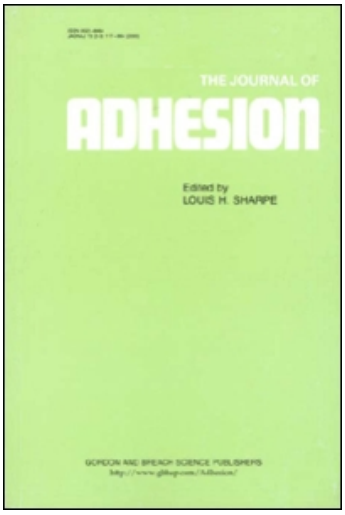

The Journal of Adhesion

Publication details, including instructions for authors and subscription information:
http://www.informaworld.com/smpp/title~content=t713453635

Fracture Analysis of the Constrained Blister Test

Henrik Myhre Jensen[a]; Bruno Cochelin[b]
[a] Department of Solid Mechanics, The Technical University of Denmark, Lyngby, Denmark [b] LPMM, I.S.G.M.P., University of Metz lle de Saulcy, Metz, France

To cite this Article Jensen, Henrik Myhre and Cochelin, Bruno(1994) 'Fracture Analysis of the Constrained Blister Test', The Journal of Adhesion, 47: 4, 231 — 243
To link to this Article: DOI: 10.1080/00218469408027103
URL: http://dx.doi.org/10.1080/00218469408027103

J. Adhesion, 1994, Vol. 47, pp. 231–243
Reprints available directly from the publisher
Photocopying permitted by license only

Printed in the United States of America

Fracture Analysis of the Constrained Blister Test

HENRIK MYHRE JENSEN* and BRUNO COCHELIN**

**Department of Solid Mechanics, The Technical University of Denmark, DK-2800 Lyngby, Denmark*
***LPMM, I.S.G.M.P., University of Metz Ile de Saulcy, F-57045 Metz, France*

(Received November 15, 1993; in final form February 1, 1994)

The constrained blister test is analyzed in the framework of linear elastic fracture mechanics. Exact results for the energy release rate and the mode mixedness are obtained as functions of quantities which are natural to measure in the test. Effects of geometrical non-linearities and initial in-plane stresses are included. An analysis of the range of loads for which the test results in configurationally stable delamination is performed.

KEY WORDS Blister test; mixed mode fracture mechanics; configurational stability; contact analysis; buckling under contact.

INTRODUCTION

The constrained blister test for measuring the adhesion of thin films or tapes to various substrates was suggested in the mid-1980's, (a review of the early literature on the subject can be found in Chang *et al.*[1]). The geometry of the test is shown in Figure 1 where it is seen that the difference between this test and the classical blister test is the constraint from a rigid wall above the film which prevents the energy release rate to increase unbounded even under pressure controlled delamination and, thus, offers some advantages for experiments.

In the framework for fracture analysis of interfacial, thin film delamination described in Hutchinson and Suo,[2] the energy release rate and its separation into mode 1 and mode 2 can be calculated from the effective crack tip loads and M and ΔN (see below for definitions) according to

$$G = \frac{6(1-\nu^2)}{Eh^3}\left[M^2 + \frac{h^2}{12}\Delta N^2\right] \tag{1}$$

$$\tan\psi = \frac{\Delta N h \sin\omega + \sqrt{12}\, M\cos\omega}{\Delta N h\cos\omega - \sqrt{12}\, M\sin\omega} \tag{2}$$

Here, E is the elastic modulus of the film, ν is Poisson's ratio, h is the film thickness and the angle ω is tabulated in Suo and Hutchinson[3] as a function of the elastic mismatch between the film and the substrate. Above, M is the effective bending moment in the film and ΔN is the change in the membrane stress. The interpretation of the phase angle,

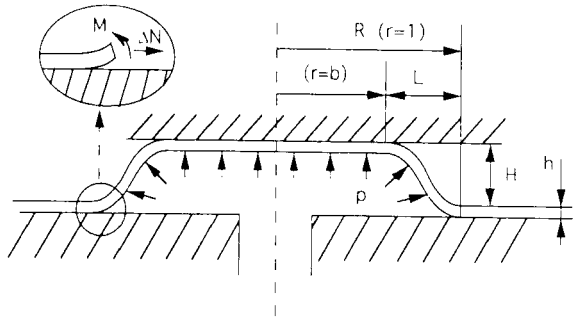

FIGURE 1 Geometry of the constrained blister test with the sign convention for the effective loads on the crack tip.

ψ, in (2) as a parameter separating mode 1 and mode 2 contributions to G has been discussed in detail in Hutchinson and Suo.[2] As a special case, in the absence of elastic mismatch, $\tan(\psi) = K_2/K_1$ and $\omega = 52.1°$. Interface fracture criteria of the type $G = G_c(\psi)$ were formulated and compared with experimental results in Jensen *et al.*[4] showing that the classical elastic fracture criterion independent of ψ is inadequate for interface debonding.

The paper will treat the constrained blister test in this formulation. At first, the axisymmetric state is discussed in the linear limit. It is shown that when the radius of the contact zone is large, *i.e.*, $1-b \ll 1$, the energy release rate reaches a steady state value $G = \text{pH}$, which is independent of the radius of the delamination, R. This steady state limit is studied in detail including effects of initial in-plane stresses and geometrical non-linearities. The effect of initial in-plane stresses is included for two reasons: Firstly, residual stresses are often present in thin film systems and have a profound influence on the behaviour of the test and, secondly, for some experimental applications, in-plane stresses are applied before loading with pressure to stabilize the test.

The experimental results obtained with the test[1] suggest that instabilities may occur at high loads in the sense that the circular delamination front becomes energetically unfavorable compared with other modes of delamination. This limits the use of the test and for this reason a stability analysis of the steady state is performed.

The purpose of this paper is to derive exact results for the crack tip quantities of interest (1) and (2) specifically for the constrained blister test and to analyze the test for stability. The results are presented as functions of the quantities which are natural to measure in experiments.

THE LINEAR AXISYMMETRIC STATE

To gain some insight into the problem, consider a circular delamination of radius R under axisymmetric deformation. The normal deflection, $w(r)$, under pressure, p, valid for small deformations is given by

$$w(r) = c_1 + c_2 \ln(r) + c_3 r^2 + c_4 r^2 \ln(r) + \frac{pr^4 R^4}{64D} \tag{3}$$

where $r(b \leq r \leq 1)$ is the distance to the centreline normalized by R and $D = Eh^3/12(1-\nu^2)$ is the bending stiffness. The constants c_i are chosen so that the boundary conditions at $r = 1$ and the contact conditions at $r = b$ are satisfied. These conditions are

$$w(1) = 0 \quad w'(1) = 0 \tag{4a}$$

$$w(b) = H \quad w'(b) = 0 \quad M(b) = 0 \tag{4b}$$

The five conditions in (4) define a system of equations in the five unknowns c_i and b, which was also formulated in Lai and Dillard.[5] The equations are linear in c_i with a non-linear relationship between the height of the constraint, H, and the radius of the contact zone, bR. From the solution of (4), the bending moment at the crack front $M = Dw''(1)/R^2$ is calculated and inserted in (1) with $\Delta N = 0$, from which the energy release rate is obtained as

$$G = \frac{p^2R^4}{16D}\left[\frac{(b^4-1)\ln(b) - (b^2-1)^2}{b^2 - 1 - 2\ln(b)}\right]^2 \tag{5}$$

with the relationship between H and b given by

$$H = \frac{pR^4}{64D}\left[\frac{b^6 - 5b^4 + 7b^2 - 3 + 2\ln(b)(3b^4 - 2b^2 - 1) - 8b^4\ln(b)^2}{b^2 - 1 - 2\ln(b)}\right] \tag{6}$$

By combination of (5) and (6) it is readily seen that $G = \mathrm{pH}f(b)$ where $f(b = 1) = 1$. A plot of G/pH is shown in Figure 2 where it is seen that the energy release rate reaches a steady state value, $G = \mathrm{pH}$, as delamination increases. In an experimental situation,

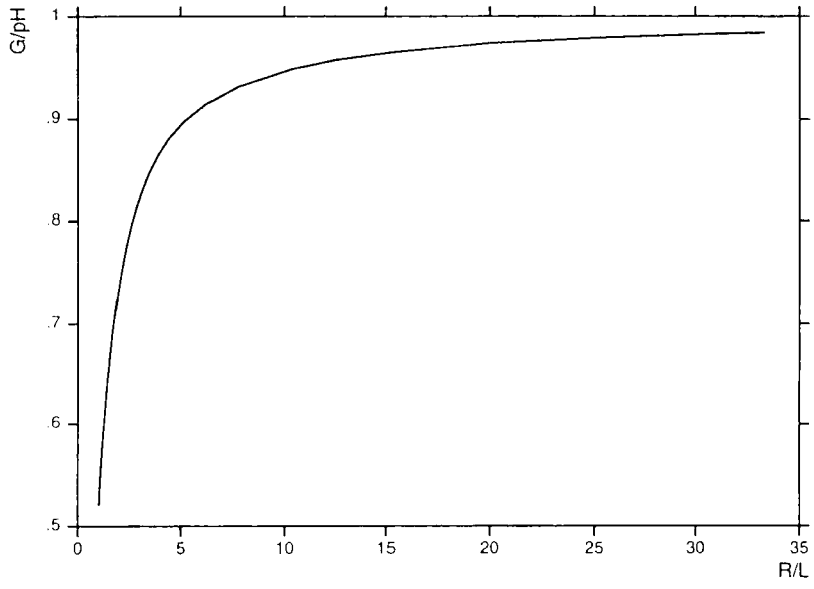

FIGURE 2 Variation of normalized energy release rate as a function of the radius of delamination normalized by its distance to the contact radius.

natural quantities to measure are p, H, R and b. From (5) and (6), one of these is not necessarily required in order to determine G.

The expansions of G and H from $b = 1$ are obtained from (5) and (6) from which

$$G \cong \mathrm{pH}\left(1 - \frac{8}{15}\frac{L}{R}\right) + O\left(\frac{L^2}{R^2}\right) \tag{7}$$

where $L = R(1 - b)$. This is a small correction to an earlier published result[1] where $G = \mathrm{pH}(1 - L/2R)$ was obtained by an approximate method. In the formulation above, it is not necessary in general to calculate G numerically as suggested in Lai and Dillard.[5]

To conclude this introductory section, the crack tip mode mixedness can be predicted from (2) as $K_2/K_1 = -0.78$ for identical elastic properties of the film and the substrate. Note that there is no restriction on the elastic constants of the film or the substrate provided they are isotropic; the assumption of identical properties is for illustration only. In the linear theory leading to (3), no change in the ratio between the mode 2 and mode 1 field at the crack tip can be predicted. The following section which takes non-linearities into account shows that this change in mode mixedness can be substantial especially in the presence of initial in-plane stresses. We will analyze the steady state limit only, so that the circular geometry at the crack front can be replaced by a plane strain Cartesian geometry.

STEADY STATE ANALYSIS

In the steady state limit, plane strain conditions hold in the circumferential direction. In the analysis of the steady state, geometrical non-linearities are included to allow the height of the constraint to be greater than the film thickness. In many thin film systems residual stresses are present and these are also included in the analysis by assuming initial values for the in-plane stresses. In the following, we refer to these as prestresses and they are assumed to act equi-biaxial.

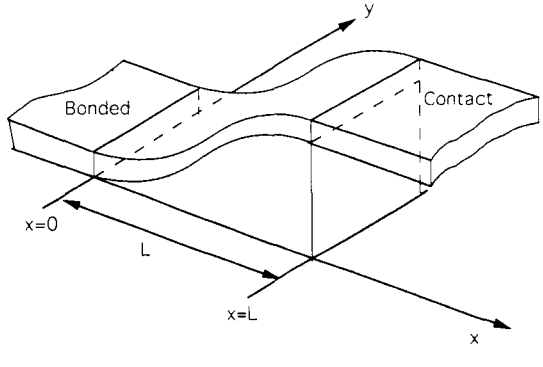

FIGURE 3 Geometry for the steady state analysis.

A Cartesian coordinate system is introduced where $x = 0$ at $r = 1$ (see Fig. 3) and $x = L$ at $r = b$. In this and the following sections, dimensionless quantities ($\tilde{}$) are introduced according to

$$\tilde{x} = \frac{x}{L} \quad \tilde{w} = \frac{w}{h} \quad \tilde{H} = \frac{H}{h} \quad \tilde{u} = \frac{uL}{h^2} \quad \tilde{v} = \frac{vL}{h^2}$$
$$\tilde{M} = \frac{ML^2}{Dh} \quad \tilde{N} = \frac{NL^2}{D} \quad \tilde{p} = \frac{pL^4}{Dh} \quad \tilde{G} = \frac{2GL^4}{Dh^2} \tag{8}$$

where u and v are the in-plane displacements in the x- and y-direction, respectively. In non-dimensional quantities, the governing von Kármán equations and boundary conditions are

$$\tilde{w}^{IV} - (\tilde{N}_0 + \Delta\tilde{N})\,\tilde{w}'' = \tilde{p}$$
$$\Delta\tilde{N} = 6\int_0^1 (\tilde{w}')^2\,d\tilde{x} \tag{9}$$
$$\tilde{w}(0) = 0 \quad \tilde{w}'(0) = 0 \quad \tilde{w}(1) = \tilde{H} \quad \tilde{w}'(1) = 0 \quad \tilde{w}''(1) = 0$$

where $\tilde{N}_0$ is the normalised prestress in the system. The solution to (9) can be obtained in closed form. In the derivation of (9), it is assumed that the deformation is plane strain in the y-direction when measured relative to the prestressed state. It is also assumed that $N_{xx}(x = L) = N_0$ which corresponds to a frictional sticking boundary condition for the in-plane displacement: $u(x = L) = 0$. Note that, due to the normalizations in (8), the distance L from the crack front to the contact zone—which is free to vary—does not enter the equations explicitly.

Below, we list the exact solutions to (9) in the two limits $p \to 0$ and $p \to \infty$ which give very simple expressions for the fundamental quantities of interest. These are given together with their approximate range of validity. The full non-linear solution is also presented in a form which can directly be applied to experimental measurements.

Solutions for Small Deformations

When the normal deformation $\tilde{w}$ is small, the stress change, $\Delta\tilde{N}$, relative to the prestress, $\tilde{N}_0$, in (9) can be neglected and the closed form solution gives the following results for the energy release rate for tensile prestresses ($\tilde{N}_0 > 0$) and compressive prestresses ($\tilde{N}_0 < 0$), respectively.

$$\tilde{G} = \tilde{p}^2 \times \begin{cases} \dfrac{(4 + t^2)\cosh(t) + t^2 - 4 - 4t\sinh(t)}{(\cosh(t) - 1)\,t^4} & t = \sqrt{\tilde{N}_0} \\ \dfrac{(4 - t^2)\cos(t) - t^2 - 4 + 4t\sin(t)}{(\cos(t) - 1)\,t^4} & t = \sqrt{-\tilde{N}_0} \end{cases} \tag{10}$$

Comparison with the full solution shows that (10) holds within 5% accuracy for $\tilde{p} \le 2(15 + \tilde{N}_0)$, at least for relatively small values of normalized prestress. Since (9) has

been linearized, the change in membrane stress is neglected and the mode mixedness remains constant at the same value as in Section 2. Note that (10) requires knowledge of the prestress which is not always easy to measure. But (10) can be reexpressed as

$$\tilde{G} = 2\ \tilde{\mathrm{p}}\tilde{\mathrm{H}} \tag{11}$$

for arbitrary signs of the prestress. The relationship in (11) does not require knowledge of the prestresses and it is identical to the limit value of (7) as $L \to 0$. Note that the factor 2 in (11) follows from the choice of normalization of G in (8).

Solutions for Large Pressure

The solution of (9) for $\tilde{p} \to \infty$ also gives simple expressions for the fundamental quantities of interest. Now,

$$\frac{\tilde{M}}{\Delta\tilde{N}} = \frac{\sqrt{2}}{2}, \quad \Delta\tilde{N} = 8\tilde{H}^2, \quad \tilde{G} = \frac{7}{3}\tilde{\mathrm{p}}\tilde{\mathrm{H}} = \frac{112}{3}\tilde{H}^4 \tag{12}$$

which is obtained as an exact limit of the full closed form solution. The results in (12) are accurate within 5% of the full solution when $\tilde{p} \geq 10^3(50\text{-}\tilde{N}_0)$ for moderate values of normalized prestress. The ratio between the bending moment and the membrane stress change reaches a constant value in this limit, and from (12) and (2), $K_2/K_1 = -1.74$ in the special case of no elastic mismatch in the system. Note from (12) that the bending moment at the boundary cannot be neglected in the membrane limit due to the development of a boundary layer, see also Jensen[6].

Buckling-Driven Delamination

In the case of a compressive prestress $N_0 < 0$ with $p = 0$, a solution to (9) will always exist since L is not limited in the formulation. In practice, L is limited by the circular geometry and sets a lower limit to the prestress at which buckling occurs. The solution to (9) again results in remarkably simple relationships between the crack tip quantities and quantities which are natural to measure for the test. Now,

$$\tilde{M} = 0, \quad \Delta\tilde{N} = 4\pi^2 - \tilde{N}_0 = 9\tilde{H}^2, \quad \tilde{G} = \frac{27}{4}\tilde{H}^4 \tag{13}$$

It is interesting to note also that, in this limit, there is no change in the phase angle of loading despite the fact that the solution is valid for arbitrary $\tilde{H}$. For $\omega = 52.1^\circ$ in (2), $K_2/K_1 = 1.28$. The change in sign of the ratio K_2/K_1, compared with the previous sections, indicates that the crack tip solutions in Ref. 3 leading to (2) no longer are valid, because $K_1 < 0$ is predicted and effects of contacting crack sides should be taken into account. The combinations of loads for which (2) is valid will be shown in Section 3.4.

Exact Solutions

The exact solution to (9) is very elaborate and it will not be reported here. Simple and useful forms of the exact solution can be obtained after observing that the integral

in (9) varies slowly from $9\tilde{H}^2$ for buckling-driven delamination to $8\tilde{H}^2$ as $\tilde{p} \to \infty$ according to (12) and (13). For tensile prestresses, the variation is even less going from $288\tilde{H}^2/35 (\approx 8.23\,\tilde{H}^2)$ for small pressure to $8\tilde{H}^2$ as $\tilde{p} \to \infty$. The explanation for the integral being nearly constant is the limited possibility for the normal deflection to change under the boundary and contact conditions (9). In Figure 4, all possible normal deflections are shown between the two extremes; buckling-driven delamination, and the membrane limit which is obtained as $\tilde{p} \to \infty$.

In order to determine the bending moment, $\tilde{M}$, at the crack front so that the crack tip quantities (1) and (2) can be calculated, the residual stress in the system, $\tilde{N}_0$, must be known. If it cannot be measured directly, the curves obtained from the exact solution of (9) shown in Figure 5 can be combined with measurements of pressure, constraint height and the distance L Knowing the residual stress, the bending moment is calculated from the exact solution

$$\tilde{M} = 2\tilde{H}s^2 \times \begin{cases} \dfrac{-1}{2 + s\sinh(s)/(1-\cosh(s))} & \text{tension} \\ \dfrac{1}{2 - s\sin(s)/(1-\cos(s))} & \text{compression} \end{cases} \tag{14}$$

where $s = \sqrt{|\tilde{N}_0 + \Delta\tilde{N}|}$. The separation between the region with compression and the region with tension is obtained by solving (9) with $\tilde{N}_0 + \Delta\tilde{N} = 0$. From this, the blister is

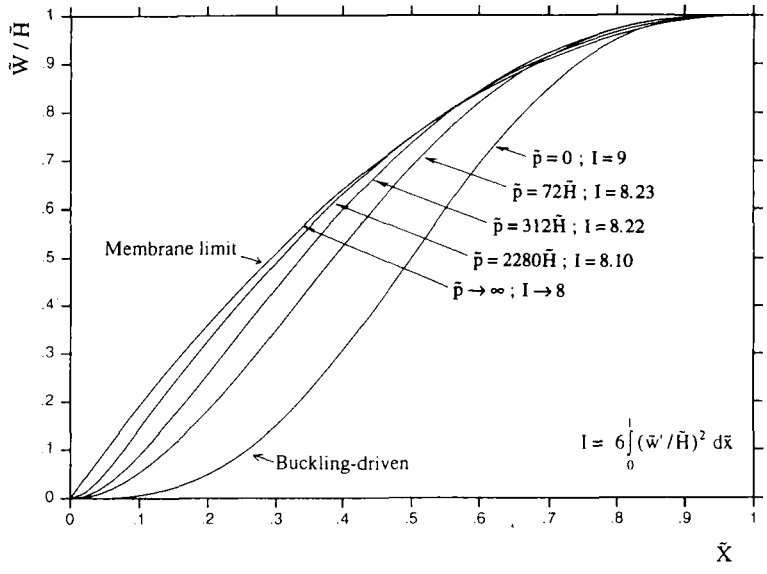

FIGURE 4 Variation of normal deflection of the blister between the crack front and the contact zone at various load conditions.

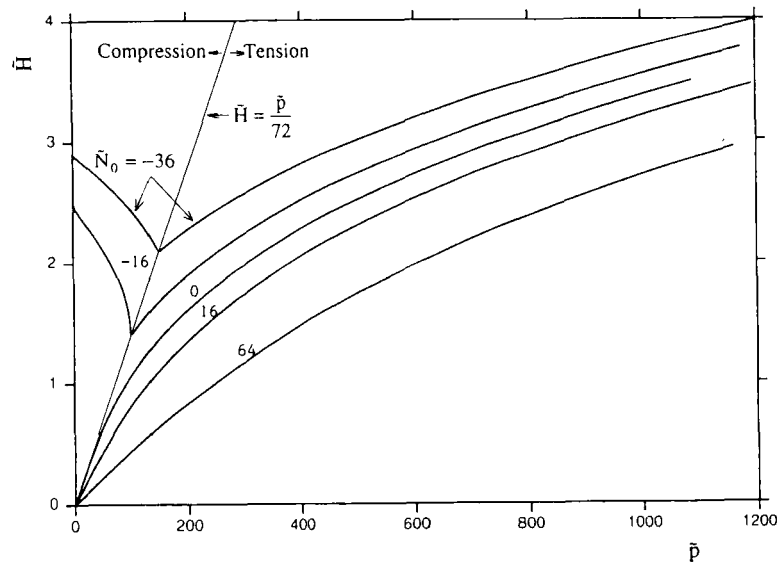

FIGURE 5 Constraint height as a function of pressure from which the prestress can be determined.

in tension if:

$$\tilde{H} \leq \tilde{p}/72 \quad \text{from which}$$
$$\Delta\tilde{N}/\tilde{M} \leq 105\,\tilde{p} \quad \text{and} \quad \tilde{G} \leq 144\,\tilde{H}^2\left(1 + \frac{48}{1225}\tilde{H}^2\right) \tag{15}$$

It does not seem to be possible to avoid measuring the prestress or to estimate it from Figure 5 in order to determine the bending moment.

The denominator in (2) is zero for $\Delta\tilde{N} - \sqrt{12}\,\tilde{M}\,\tan\omega = 0$ and the present analysis holds for $\Delta\tilde{N} - \sqrt{12}\,\tilde{M}\,\tan\omega < 0$, only, since this implies that $K_1 > 0$[2]. Otherwise, effects of contacting crack sides should be included in the analysis Figure 6 shows the region where (2) is valid for $\omega = 52.1^\circ$ corresponding to no elastic mismatch in the system. In this region, the ratio of stress change to bending moment is shown in Figure 7 which is obtained from the exact solution. From Figure 7, the phase angle of loading, ψ, at the crack tip can be obtained for any elastic mismatch using (2) with the appropriate value of ω from Ref. 3. It is clearly seen that the presence of prestresses in the blister can significantly change the phase angle of loading, ψ, at the crack tip.

The presence of prestresses also has a significant influence on the energy release rate as shown in Figure 8. For completeness, the plots in Figures 6–8 include the regions where the stress in the blister is compressive with the separation between the tensile and compressive zones as given by (15) included.

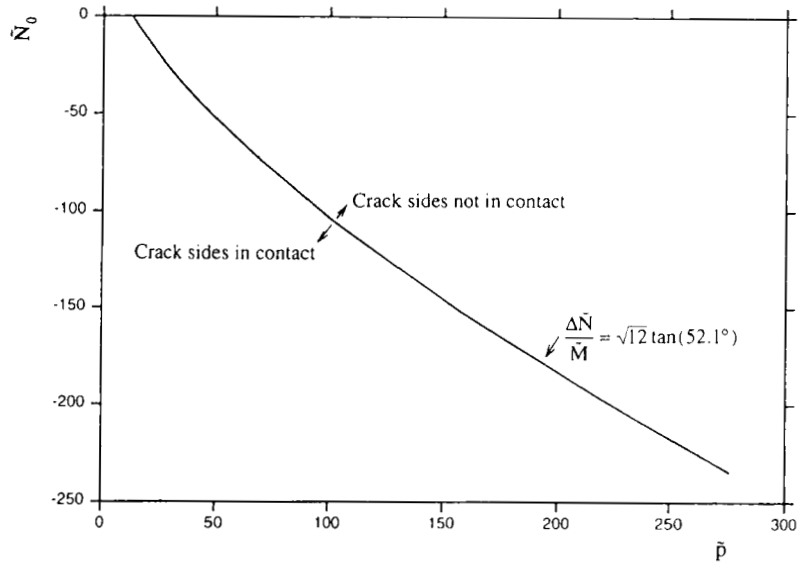

FIGURE 6 Region where $K_1 > 0$ in the case of no elastic mismatch in the system. Note that the prestress and the pressure are normalised according to (8).

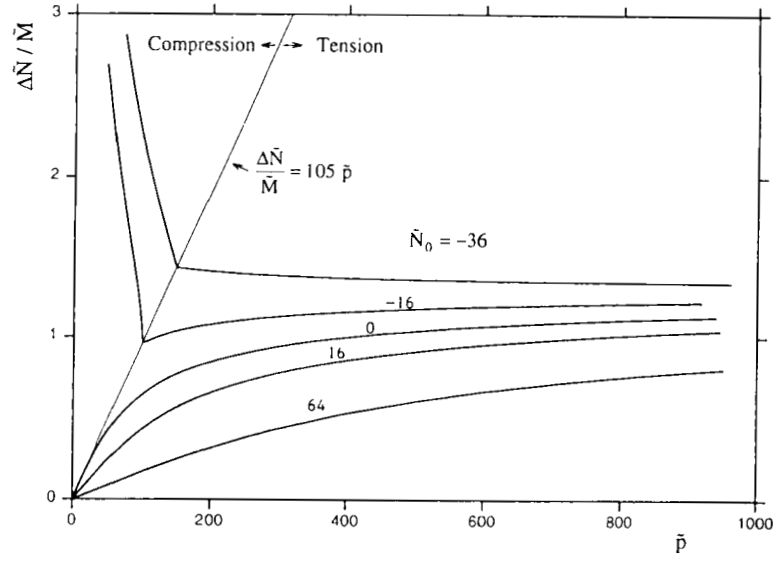

FIGURE 7 Ratio of effective crack tip loads from which the mode mix can be obtained using (2).

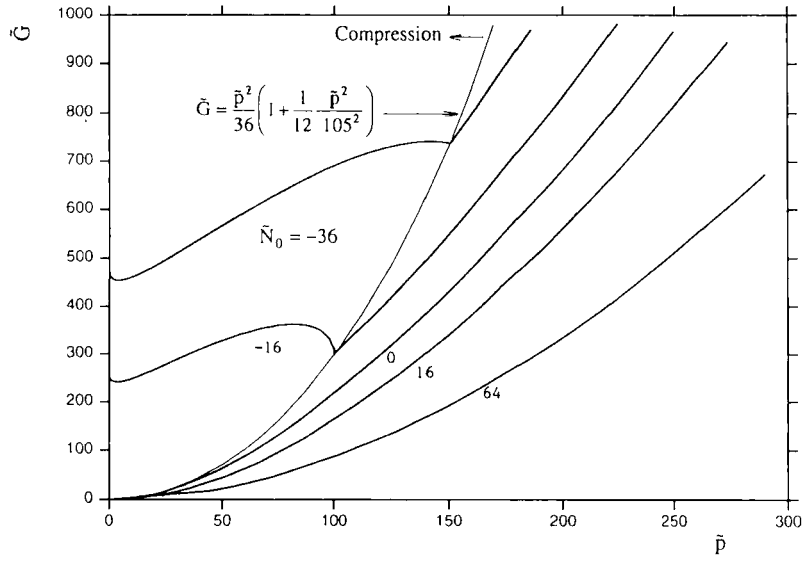

FIGURE 8 Energy release rate as a function of pressure for different levels of prestress.

CONFIGURATIONAL STABILITY

A phenomenon which may affect the applicability of the constrained blister test is the possible evolution of non-axisymmetric crack growth. Such non-symmetries may result from bifurcations in the delaminated regions or from energetically more favorable crack front morphologies than the circular shape.[7-9] The purpose of the following section is to show the range of loading parameters for which the constrained blister test is stable in this sense.

A small perturbation of the crack front as sketched in Figure 9 is introduced. In non-dimensional quantities, the plate equations governing the perturbation problem are

$$\tilde{w}_1^{IV} - (2\tilde{k}^2 + \tilde{N}_{xx})\tilde{w}_1'' + \tilde{k}^2(\tilde{k}^2 + \tilde{N}_{yy})\tilde{w}_1 = 12\tilde{w}''(\tilde{u}_1' + \tilde{w}_1'\tilde{w}' + \nu\tilde{k}\tilde{v}_1)$$

$$(\tilde{u}_1' + \tilde{w}_1'\tilde{w}' + \nu\tilde{k}\tilde{v}_1)' + \frac{1-\nu}{2}\tilde{k}(\tilde{v}_1' - \tilde{k}(\tilde{u}_1 + \tilde{w}_1\tilde{w}')) = 0 \tag{16}$$

$$\frac{1-\nu}{2}(\tilde{v}_1' - \tilde{k}(\tilde{u}_1 + \tilde{w}_1\tilde{w}'))' - \tilde{k}(\tilde{k}\tilde{v}_1 + \nu(\tilde{u}_1 + \tilde{w}'\tilde{w}_1')) = 0$$

where $\tilde{k} = 2\pi L/\lambda$ and λ is the perturbation wavelength. The normal deflection of the blister, $\tilde{w}(\tilde{x})$, entering (16) is known from the solution in Section 3.4 and for completeness this function is given in the Appendix. The boundary conditions at $\tilde{x} = 0$ derived by methods similar to the analysis in Hutchinson *et al.*[7] and Jensen[10] are

$$\tilde{u}_1 = -\frac{\Delta\tilde{N}}{12} \quad \tilde{v}_1 = 0 \quad \tilde{w}_1 = 0 \quad \tilde{w}_1' = -\tilde{M} \tag{17}$$

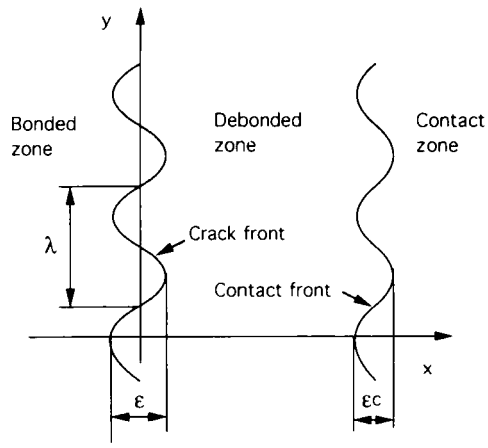

FIGURE 9 Conventions for the perturbation analysis. The crack front is perturbed by $\varepsilon\cos(\tilde{k}y/L)$ and the perturbation of the contact zone following this is $c\,\varepsilon\cos(\tilde{k}y/L)$ with c determined as a part of the solution.

where $\Delta\tilde{N} \cong 8\tilde{H}^2$ (cf. Section 3.4 and Fig. 4) and $\tilde{M}$ is given by (14). A consequence of the crack front perturbation is, in general, a perturbation of the contact zone. The amplitude of the contact perturbation is unknown and has to be determined as a part of the solution. The contact conditions at $\tilde{x} = 1$ are given by

$$\tilde{u}_1 = -c\frac{\Delta\tilde{N}}{12} \quad \tilde{v}_1 = 0 \quad \tilde{w}_1 = 0 \quad \tilde{w}_1' = 0 \quad \tilde{w}_1'' = -c\tilde{w}''' \tag{18}$$

where the last condition at $\tilde{x} = 1$ ensures that the contact condition $M = 0$ is not broken along the perturbed contact zone. The unknown c appearing in (18) determines the ratio between the amplitudes of the contact zone perturbation and the crack front perturbation indicated in Figure 9. As for the axisymmetric problem in Section 2 and the steady state problem in Section 3, one more boundary condition than for conventional problems is obtained reflecting that the extend of the contact area is unknown *a priori*.

Next, from the solution of (16)–(18), the energy release rate and phase angle of loading can be calculated along the perturbed crack front and compared with the quantities on the straight front. The shape of the crack is then given by choosing the mode which releases most energy at the crack tip. This criterion for choosing the most stable mode is dependent on what interface fracture criterion is imposed. In the simplest form, the most energetically favorable mode of delamination has a value of $\tilde{k}$ for which

$$\begin{aligned}&(\Delta\tilde{N} - \tan\omega\sqrt{12}\,\tilde{M})(12\,\tilde{u}_1' - \tan\omega\sqrt{12}\,\tilde{w}_1'') + \\ &\Gamma(\Delta\tilde{N}\tan\omega + \sqrt{12}\,\tilde{M})(12\,\tilde{u}_1'\tan\omega + \sqrt{12}\,\tilde{w}_1'') = \text{minimum}\end{aligned} \tag{19}$$

where Γ can vary between 0 and 1 with these two extremes corresponding to a fracture criterion where $K_1 = K_c$ independent of K_2 and the classical Griffith criterion $G = G_c$ independent of K_1/K_2, respectively. A micromechanical model where these two

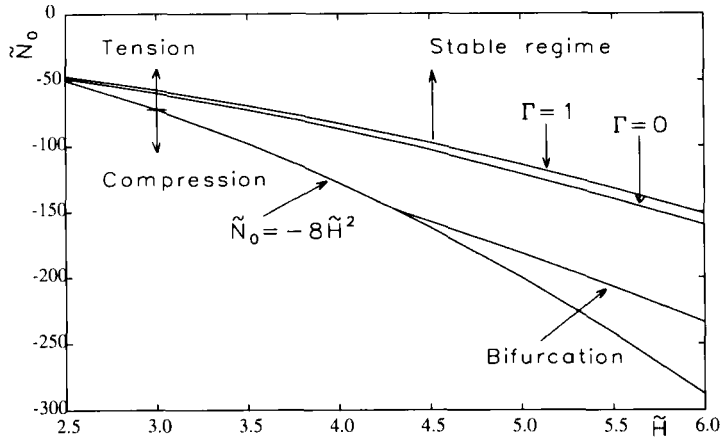

FIGURE 10 Stability map for the constrained blister test showing combinations of prestress and height of the constraint for which the test results in configurationally stable delamination.

fracture criteria apply for rough and smooth interfaces, respectively, was analysed in Evans and Hutchinson.[11] The straight crack front is stable if the minimum in (19) is reached for $\tilde{k} = 0$.

The system of ordinary differential equations (16) under the boundary equations (17) and (18) are integrated numerically using a standard Runge–Kutta procedure. The integration is performed as an initial value problem from $\tilde{x} = 0$ to $\tilde{x} = 1$ so that a linear set of equations in the five unknowns c, $\tilde{w}_1''(0)$, $\tilde{w}_1'''(0)$, $\tilde{u}_1'(0)$, $\tilde{v}_1'(0)$ is obtained from the five boundary conditions at $\tilde{x} = 1$ in (18). During the stability analysis, the sign of the determinant of this linear system is checked. The zeroes of the determinant correspond to buckling of the deformed plate under the contact conditions with the wall (18).

Numerical results of the stability analysis are summarized in Figure 10 where combinations of prestress and height of the constraint leading to instability and bifurcation are shown. Only tensile stresses in the delaminated region are considered. For $\tilde{H} < \sim 2.5$, the constrained blister test results in configurationally stable delamination. For $\tilde{H} > 2.5$, instabilities in the shape of the crack front may occur for sufficiently large compressive prestresses. From Figure 10 it is possible to read off how large a tensile stress there has to be superimposed on compressive prestresses to stabilize the test. The bifurcations in the system occur with $\lambda \approx L$ in the range of parameters in Figure 10.

CONCLUSION

The constrained blister test was analysed in the context of linear elastic fracture mechanics. Exact results for the crack tip energy release rate and mode mixedness valid for arbitrary elastic mismatch between the film and the substrate were derived. The axisymmetric state was analysed in the linear limit, while the steady state was analysed

more rigorously. In the steady state analysis, the circular geometry was replaced by a Cartesian geometry with a straight crack front. Effects of initial in-plane stresses and geometrical non-linearities were included. A stability analysis was carried out to investigate the range of loads for which the constrained blister test is useful in the sense that the straight crack front is the most energetically favorable mode of delamination. The stability analysis included, as a special case, a bifurcation analysis of a finitely deformed plate in unilateral contact with a wall.

Acknowledgements

Support from The University of Metz and The Danish Technical Research Council is gratefully acknowledged.

References

1. Y.-S. Chang, Y.-H. Lai and D. A. Dillard, *J. Adhesion*, **27**, 197–211 (1989).
2. J. W. Hutchinson and Z. Suo, *Adv. Appl. Mech.*, **29**, 63–191 (1990).
3. Z. Suo and J. W. Hutchinson, *Int. J. Fracture*, **43**, 1–18 (1990).
4. H. M. Jensen, J. W. Hutchinson and K. -S. Kim, *Int. J. Solids Structures*, **26**, 1099–1114 (1990).
5. Y.-H. Lai and D. A. Dillard, *J. Adhesion*, **31**, 177–189 (1990).
6. H. M. Jensen, *Eng. Fract. Mech.*, **40**, 475–486 (1991).
7. J. W. Hutchinson, M. D. Thouless and E. G. Liniger, *Acta Metall. Mater.*, **40**, 295–308 (1992).
8. H. M. Jensen and M. D. Thouless, *Int. J. Solids Structures*, **30**, 779–795 (1993).
9. H. M. Jensen and M. D. Thouless, "Buckling instability of straight edge cracks" (submitted to J. Appl. Mech.).
10. H. M. Jensen, *Acta Metall. Mater.*, **41**, 601–607 (1993).
11. A. G. Evans and J. W. Hutchinson, *Acta Metall. Mater.*, **37**, 909–916 (1989).

APPENDIX

In this Appendix, for completeness, we list the expression for the normalised deflection $\tilde{w}$ from the exact solution of (9) which enters the perturbation equations (16)–(18). The solution is shown only for a state of tension in the blister. Note, as given by (15), that this can also be the result of compressive prestresses provided the pressure is sufficiently high. The deflection is

$$\tilde{w} = a\left(\frac{\cosh(s\tilde{x}) - 1}{s^2}\right) + b\left(\frac{\sinh(s\tilde{x}) - s\tilde{x}}{s^3}\right) - \tilde{p}\left(\frac{\tilde{x}^2}{2s^2}\right) \tag{A1}$$

where

$$a = \frac{2\tilde{H}\alpha_2 s^2}{\alpha_4 - 2\alpha_2} + \frac{\tilde{p}}{s^2} \quad b = \frac{-\alpha_4 \tilde{H} s^2}{\alpha_4 - 2\alpha_2} - \frac{\tilde{p}}{2} \quad \alpha_2 = \frac{\cosh(s) - 1}{s^2}$$

$$\alpha_4 = \frac{\sinh(s)}{s} \quad \tilde{p} = \frac{-\tilde{H}\alpha_2 s^4}{2\alpha_4(1 - s^2) - 1 - 2\alpha_2} \tag{A2}$$

$$s = \sqrt{\tilde{N}_0 + \Delta\tilde{N}} \; (\tilde{N}_0 + \Delta\tilde{N} \geq 0)$$